

TIG Welding of Sintered AISI 316 L Stainless Steel

Maurício David Martins das Neves^{1, a}, Luzinete Pereira Barbosa^{1, b}
Luis Carlos Elias da Silva^{1, c}, Olandir Vercino Correa^{1, d}, Isolda Costa^{1, e}
¹ Instituto de Pesquisas Energéticas e Nucleares, IPEN/CNEN-SP, CCTM
Av. Prof. Lineu Prestes, 2242 CEP 05508-000 SP-SP, Brasil
^a mdneves@ipen.br; ^b luzinete@ipen.br, ^c lcesilva@ipen.br, ^d ovcorrea@ipen.br and ^e icosta@ipen.br

Keywords: Welding, stainless steel sintered, AISI 316 L

Abstract. Stainless steel (SS) powders are used in the preparation of sintered SS products. One of the applications of sintered SS products is as filters in the petrochemical and food processing industries. In these industries, the SS filters are subject to severe conditions associated with the removal of solid particles from the fluid. Hence, SS filters should have adequate mechanical strength and high corrosion resistance. Welding can be used to manufacture SS filters. In this study, sintered AISI 316L specimens were welded using the TIG (Tungsten Inert Gas) process. The weld joints were examined by optical microscopy and by scanning electron microscopy. Electrochemical polarization measurements were carried out to evaluate the influence of welding on the corrosion resistance of sintered filters.

Introduction

Some papers on welding of low density sintered filters, using the TIG process, reported results that these were adequate for certain applications [1-8]. Nevertheless, some problems related to welding of sintered products were also reported [4,5].

Alterations in physical properties, mainly conductivity and thermal expansion, of sintered products, lead to heterogeneous behavior during welding. Variation in thermal conductivity alters heat transfer, where as variations in thermal expansion coefficient, due to melting of the powder and ingress of liquid metal in the pores, causes dimensional changes. Impurities from the pores that are not removed during sintering can also cause erratic arc behavior. This could alter the welding conditions and the corrosion resistance.

This paper presents the influence of TIG welding parameters on the corrosion resistance of sintered AISI 316 L stainless steel weld joints.

Materials and Methods

Water atomized AISI 316L stainless steel powders with grain size in the range 100 to 200 μm were used in this study. These powders are used in the manufacture of plates and cylindrical pieces. The chemical composition of the base material (BM) and the weld metal (WM) as well as the apparent density (AD) and flowability (f) are shown in table 1.

Table 1: Chemical composition of BM and WM as well as flowability and apparent density of BM.

	%C	%Cr	%Ni	%Mo	%Si	%Fe	AD [g/cm ³]	f [s/50g]
BM	0.03	16.6	12.40	2.30	1.0	Bal.	2.09	49.2
WM	0.03	18.50	12.50	2.50	0.9	Bal.	-	-

The powders were axially cold compacted at pressures of 100 and 300 MPa. These compacts were sintered in a vacuum furnace at 1260 °C for 1 hour at 3.10^{-5} torr. The density of the sintered BM used for welding was in the range 4.20 to 4.50 g/cm³.

The sintered plates and small tubes were positioned in devices designed for carrying out longitudinal and circumferential welds. Linear welding of the plates and circumferential welding of the tubes were carried out since larger pieces are manufactured using similar processes.

Tungsten inert gas (TIG) welding of the sintered plates and tubes was carried out on specimens with butt joints and without a gap at the joint. The welds were carried out with and without the use of weld metal (WM).

Tables 2 and 4 show the main welding parameters and the influence of these parameters on weld geometry. The other parameters were maintained constant during the welding process. These included: composition of tungsten with 2% of ThO₂, rod diameter of 1.0 mm and pure argon as the protective gas with a flow rate of 20 l/min. The weld metal (WM), when used was AWS E316L rod with 1.6 mm diameter.

The microstructure of the weld joint was examined for discontinuities in an optical microscope (Olympus BX 60M) and in a scanning electron microscope (Philips XL 30) The welded specimens were tensile tested in an INSTRON 4400R universal testing machine. The fracture regions were examined in a SEM.

Potentiodynamic polarization measurements were carried out with weld joint specimens in 100 mM NaCl to determine the influence of welding parameters on the corrosion resistance of the sintered specimens. The polarization measurements were carried with a Princeton Applied Research (PAR) EG and G mod 273 potentiostat using a 0.5 mV/s scan rate over the range -0.5 to 1.0 V.

Results and Discussion

The parameters used to weld the sintered plates and the geometries of the bead weld are shown in table 2. Specimen 1 was welded without the addition of weld metal (WM), where as specimens 2 to 13 were welded with WM.

The width of the weld was directly proportional to the welding voltage. Specimens with a large volume of molten metal in the weld zone were those welded using higher current. The influence of welding parameters on weld geometry (penetration and depth) of specimens with and without WM was similar.

Figure 1a reveals a thin weld zone of a specimen without WM addition, compared to the base metal (BM). This caused the formation of discontinuous regions. The discontinuities contribute to increase in stress concentration at the weld joint.

In figure 1b, welded with WM, the weld was totally filled. Consequently the bead joint is quite level, between the base metal surface and the weld. Weld penetration was total across the thickness of the sintered plates and regions with stress concentrations were not observed.

Table 2: Welding parameters and bead weld geometry

Specimen	Current [A]	Voltage [Volt]	Velocity [cm/min]	Penetration [mm]	Width [mm]	Face reinforcement (mm)
1	28	24	11	2.2 \pm 0.1	3.0 \pm 0.1	0.05 \pm 0.10
2	38	16	11	1.8 \pm 0.1	3.3 \pm 0.1	0.35 \pm 0.10
3	42	16	11	1.4 \pm 0.3	4.0 \pm 0.1	-0.90 \pm 0.10
4	40	16	13	1.4 \pm 0.1	3.8 \pm 0.1	0.25 \pm 0.10
5	28	24	13	1.2 \pm 0.2	3.1 \pm 0.1	0.35 \pm 0.10
6	48	15	13	2.5 \pm 0.1	5.3 \pm 0.1	0.06 \pm 0.10
7	50	15	13	2.6 \pm 0.1	4.7 \pm 0.1	1.00 \pm 0.10
8	38	16	11	2.4 \pm 0.1	3.3 \pm 0.1	1.30 \pm 0.10
9	38	16	11	2.0 \pm 0.1	3.6 \pm 0.1	1.35 \pm 0.10
10	25	25	5	1.9 \pm 0.1	4.5 \pm 0.1	0.40 \pm 0.10
12	30	20	5	2.8 \pm 0.1	5.5 \pm 0.1	0.00 \pm 0.10
13	35	23	11	2.6 \pm 0.2	3.3 \pm 0.1	0.30 \pm 0.10

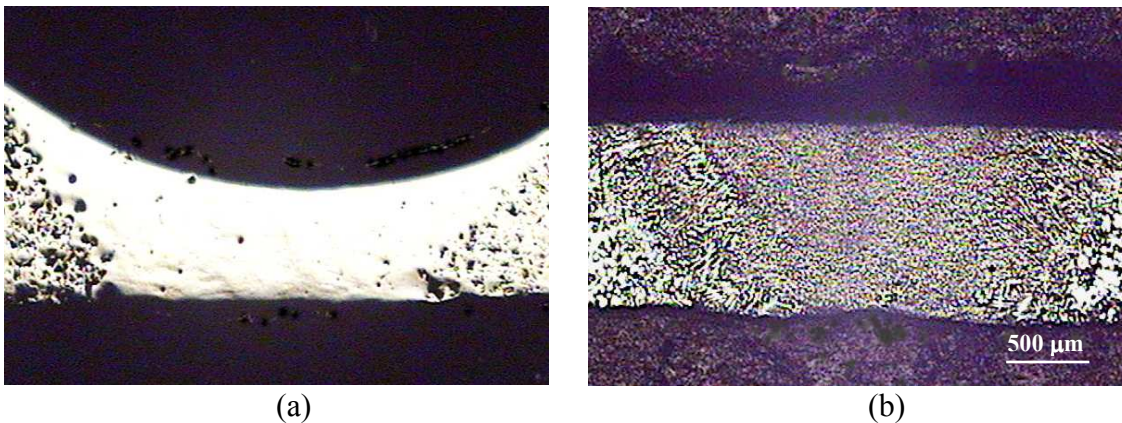


Figure 1: Optical micrographs of the weld joint. (a) without weld material and (b) with weld material.

Conditions 6, 7, 12 and 13 reveal increased weld penetration. Conditions 6 and 7 were welds prepared with higher currents and resulted in increased penetration, even at the higher welding speeds (13 cm/min). Condition 12 and 13 also resulted in higher weld penetration even though the welding speed was lower.

The use of lower welding speeds is known to result in a large heat affected zones (HAZ) in sintered products, and this could contribute towards the lowering of corrosion resistance.

Table 3 presents the average values of results obtained in the tensile tests with BM and the sintered plate welds. Comparison of the tensile test results reveals that the resistance to yield and to rupture was lower for the welded specimens, compared to BM. Reduction in the tensile test properties of the welded specimens is due to the presence of discontinuities and the residual stresses caused by welding.

The use of WM permits joints to be obtained with weld zone (WZ) dimensions similar to the thickness of the BM. That is, without significant decrease in the thickness of the WZ, as mentioned earlier. Under these conditions the welds have total penetration. The resistances to yield and to rupture are significantly higher compared to the values obtained without WM. The absence of discontinuities (stress concentrators) improves the tensile behavior of the weld joint.

The fracture surface of tensile tested BM specimens revealed regions with microcavities and these coincide with sinter neck regions and pores formed during sintering. The fracture surface reveals brittle fracture regions and plastic deformation was not observed at these regions.

Figure 2 reveals the fracture surface of a weld joint of a specimen welded without WM. The tensile tested specimens reveal fracture in the HAZ. This result confirms that besides the presence of residual stresses, a microstructure with pores and a small area of sinter necks to withstand the residual stresses contributed towards fracture in the HAZ. The fracture region of specimens welded with weld material is similar to that observed in figure 6. The presences of pores in the sintered specimens also contribute towards general reduction in mechanical properties of the specimens.

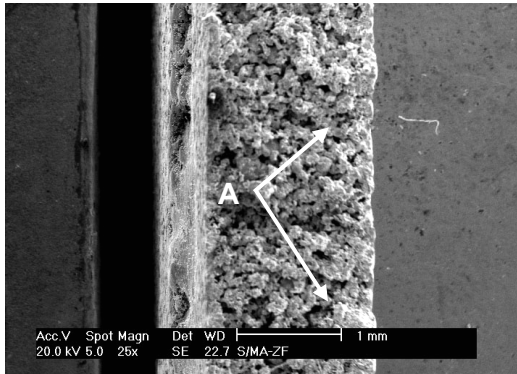


Figure 2: SEM image of specimen without MA (detail "A" stress concentrators).

Table 3: Average values of yield and ultimate tensile strength of welds.

	Yield strength [MPa]	UTS [MPa]
MB	44+2	57+4
Without MA	12+3	18+3
With MA	30+5	36+5

Table 4 shows the welding parameters used to weld cylindrical specimens and the dimensions (penetration and width) of the weld. Increase in current intensity increased WZ volume, aiding increased weld penetration and weld width. Higher welding speeds reduced the WZ, causing decrease in weld penetration and weld fillet width. Longer arcs increased width and decrease weld penetration.

Table 4: Welding parameters and weld dimensions.

Specimen	Current [A]	Polarity	Velocity [cm/min]	Flow rate [l/min]	Arc length [mm]	Penetration [mm]	Width [mm]
1	20	CCPD	11.3	20	2	1.04+0.10	4.0+0.1
2	20	CCPD	11.3	20	4	0.91+0.10	4.5+0.1
3	15	CCPD	11.3	20	2	0.80+0.10	4.0+0.1
4	25	CCPD	11.3	20	2	1.06+0.10	4.3+0.1
5	20	CCPD	11.3	20	1	1.06+0.15	4.2+0.1
6	15	CCPD	11.3	20	1	0.91+0.08	3.9+0.1
7	25	CCPD	11.3	20	1	1.11+0.10	3.9+0.1
8	20	CCPD	14.1	20	2	1.02+0.20	3.9+0.1
9	25	CCPD	14.1	20	2	1.04+0.25	3.9+0.1
10	30	CCPD	14.1	20	2	1.29+0.30	4.5+0.1
11	35	CCPD	14.1	20	2	1.34+0.25	4.6+0.1

Figure 3 shows the microstructure of the weld zone (WZ) and the WZ/HAZ interface. The WZ has a fine grained structure, due to the higher cooling rate. The morphology of the WZ could be dendritic or cellular with dendritic-cellular transition regions. The different morphologies are due to variations in the cooling rates and temperature gradients. The microstructure of the WZ also depends on the ratio of elements that stabilize the austenite and the ferrite phase, as per the Schaeffler diagram.

In the HAZ close to the interface with the WZ, grain boundary melting can be observed. These regions are preferred sites for hot crack nucleation due to the presence of segregated low melting point phases. Under these conditions the grain boundary is probably not ductile enough to

withstand residual stresses. The HAZ phase continued to reveal the austenite phase formed during sintering.

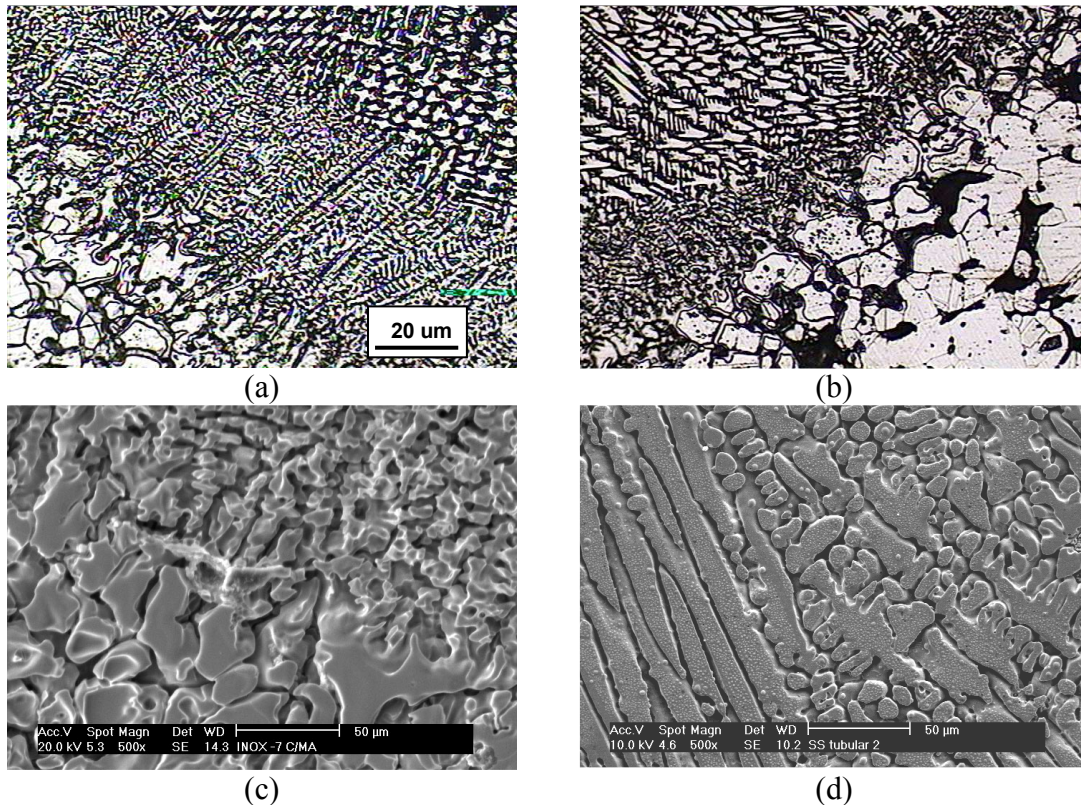


Figure 3: (a), (b) Optical micrographs, (c), (d) scanning electron micrographs of the WZ/HAZ interface.

Figure 4 compares the electrochemical polarization curves of the different specimens and the un-welded sintered 316L stainless steel had the highest corrosion resistance. This material was passive at the corrosion potential and up to 0.25V, where passive film breakdown occurred. Current oscillations that are typical of pit nucleation were observed at potentials close to 0 V. Welding caused the corrosion potential to decrease and the current densities to increase, revealing the deleterious effect of welding on the corrosion resistance of the joint.

Welding caused depolarization of the anodic reaction and this reaction is facilitated in stainless steel welded without WM. Even though the current densities of the welded specimens were very low at the corrosion potential, typical of passive materials, a rapid increase in current even at low overvoltages was observed. This indicated low resistance of the passive film on these specimens. Comparison of only the welded specimens, the results indicated that WM additions caused less reduction in corrosion properties of the stainless steels.

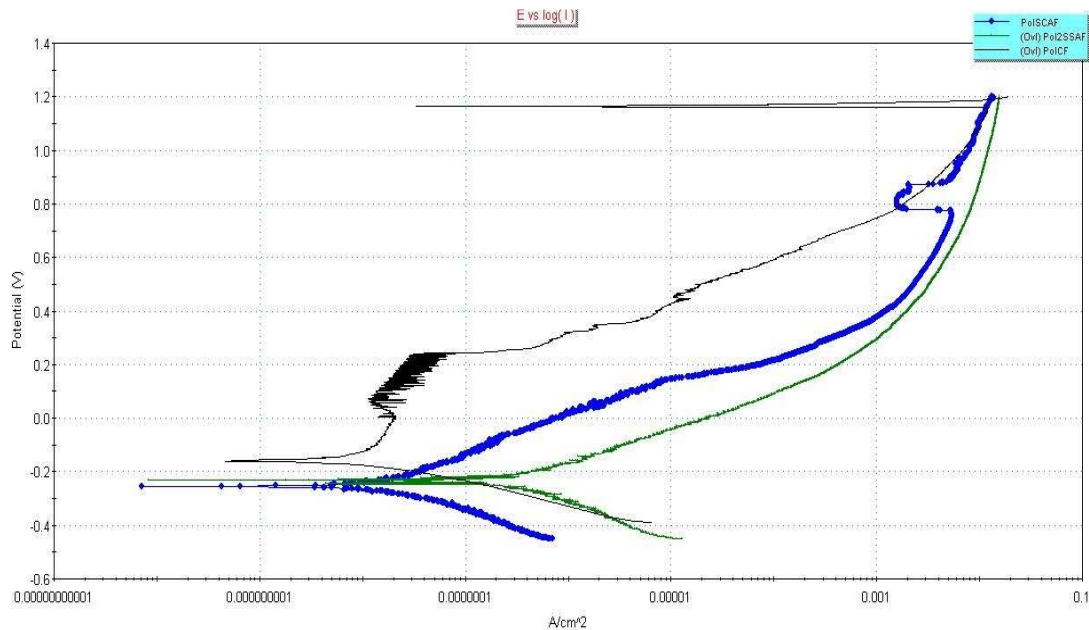


Figure 4: Potentiostatic polarization curves of specimens: Black line () standard (sintered but not welded, blue () with WM and green () without WM.

Conclusions

Welding of sintered plates without the use of weld material can lead to formation of notches and result in lowered mechanical strength.

Filters with tubular geometry can be welded without WM. Even with incomplete penetration this is a viable option.

Welding of sintered filters causes loss of protective passive film properties and decrease in corrosion resistance.

References

1. Metals Handbook, Powder Metallurgy – ASTM, 9^a Ed., 4, 1993
2. C. R. F. Azevedo: Engineering Failure Analysis Vol. 12 (2005), p. 167.
3. R. M. German: Powder Metallurgy of Iron and Steel (John Wiley & Sons Inc, 1st Ed. New York, N.Y., 1998).
4. J. A. Hamill, F. R. Manley and D. E. Nelson: Fusion welding P/M components for automotive applications, SAE Technical Paper 930490, Detroit-Mi, EUA, March, 1993.
5. Hamill, Jr. and A. Jack: The International Journal of Powder Metallurgy Vol. 37 (7) (2001), p.41.
6. M. D. M. Neves: Soldagem de Aços Inoxidáveis AISI 316 L Sinterizados pelo Processo GTAW, XXXII CONSOLDA, 2006, Belo Horizonte – MG, Brasil
7. K. Couchman, M. Kesterholt and R. White: Metal Powder Industries Federation, June (1988), p. 33.
8. G. W. Halldin, S. N. Patel, and G. A. Duchon: Progress Powder Metall. Vol. 39 (1984), p. 267.

Advanced Powder Technology VII

doi:10.4028/www.scientific.net/MSF.660-661

TIG Welding of Sintered AISI 316 L Stainless Steel

doi:10.4028/www.scientific.net/MSF.660-661.454